

Modeling the Formation of Clouds in Brown Dwarf Atmospheres

Curtis S. Cooper¹, David Sudarsky², John A. Milsom³ Jonathan I. Lunine¹, Adam Burrows²

ABSTRACT

Because the opacity of clouds in substellar mass object (SMO) atmospheres depends on the composition and distribution of particle sizes within the cloud, a credible cloud model is essential for accurately modeling SMO spectra and colors. We present a one-dimensional model of cloud particle formation and subsequent growth based on a consideration of basic cloud microphysics. We apply this microphysical cloud model to a set of synthetic brown dwarf atmospheres spanning a broad range of surface gravities and effective temperatures ($g_{surf} = 1.78 \times 10^3 - 3 \times 10^5 \text{ cm s}^{-2}$ and $T_{eff} = 600 - 1600 \text{ K}$) to obtain plausible particle sizes for several abundant species (Fe, Mg_2SiO_4 , and $\text{Ca}_2\text{Al}_2\text{SiO}_7$). The particle sizes we have thus computed range from $\sim 5 \mu\text{m}$ to over $300 \mu\text{m}$ in radius over the full range of atmospheric conditions considered. We show that modal particle sizes decrease significantly with increasing brown dwarf surface gravity. We also find that brown dwarfs with higher effective temperatures have characteristically larger cloud particles than those with lower effective temperatures. We thus conclude that it is unrealistic when modeling SMO spectra to apply a single particle size distribution to the entire class of objects.

Subject headings: atmospheres: clouds, condensation, grains: fundamental parameters — stars: low mass, brown dwarfs, substellar mass objects, L dwarfs, T dwarfs, spectroscopy, atmospheres, spectral synthesis

1. Introduction

Substellar mass objects (SMOs) are fundamentally more complex than stars because of the formation of molecules in their cool outer layers. These molecular species cause the spectra to deviate strongly from blackbody values in a multitude of spectral bands (e.g., Kirkpatrick *et al.* 1999; Leggett *et al.* 1999; and Burrows *et al.* 1997). Because of the complex chemistry occurring in their

atmospheres, therefore, a comprehensive theory of SMOs requires a detailed knowledge of the opacities of all the abundant molecular species. Obtaining complete opacity data has been a major challenge for the field of SMO spectral synthesis (Burrows *et al.* 2001).

The chemistry of brown dwarf and giant planet atmospheres is further complicated by the condensation of gaseous molecules into liquid or solid cloud particles, a process which occurs naturally at low temperatures. Because clouds significantly affect spectral features, a satisfactory theory for the structure of substellar atmospheres must address cloud particle formation and subsequent growth. Detailed knowledge of the distribution of particle sizes near the photosphere is a basic requirement for properly modeling the optical ef-

¹Department of Planetary Sciences and Lunar and Planetary Laboratory, The University of Arizona, Tucson, AZ 85721; curtis@lpl.arizona.edu, jlunine@lpl.arizona.edu

²Department of Astronomy and Steward Observatory, The University of Arizona, Tucson, AZ 85721; burrows@jupiter.as.arizona.edu, sudarsky@as.arizona.edu

³Department of Physics, The University of Arizona,

fects of clouds (Lunine *et al.* 1989; Ackerman & Marley 2001).

Clouds influence brown dwarf and giant planet spectra in several important ways. First, cloud formation can deplete the atmosphere of refractory elements that become sequestered in condensed form and then rain out from the upper atmosphere. This effect is hypothesized to be important for the interpretation of the L to T dwarf spectral transition (Burrows & Sharp, 1999; Burrows *et al.* 2001). Second, clouds near the photosphere will have the general effect of smoothing out prominent spectral features (Jones & Tsuji 1997). Third, the optical albedo of irradiated objects will be increased substantially by the presence of clouds (Sudarsky *et al.* 2000).

Clouds may be manifest in brown dwarf spectra in a more subtle way. Bailer-Jones & Mundt (2000) reported photometric I-band variability of up to 7% in L dwarf spectra. The effect is a possible signature of variations due to the patchiness of clouds. Unfortunately, cloud patchiness in SMOs is not well understood because it depends on unknown meteorological details. Three-dimensional cloud models containing detailed prescriptions for convection have not yet been developed for substellar atmospheres.

In this paper, we reiterate the general conclusion arrived at in Lunine *et al.* (1989) and Ackerman & Ackerman & Marley (2001): it is not satisfactory when modeling brown dwarf spectra to assume *a priori* a single particle size distribution because the sizes of cloud particles vary strongly with effective temperature and surface gravity. We extend the previous efforts to incorporate clouds into spectral models by calculating particle sizes, based on a one-dimensional model of cloud particle growth, for several abundant species over a range of realistic atmospheric conditions. We compute particle radii spanning a broad range from about $5\ \mu\text{m}$ to over $300\ \mu\text{m}$. Therefore, in the context of this discussion, we hereafter refer to particles less than $10\ \mu\text{m}$ in radius as small; we refer to particles in the range from $10 - 100\ \mu\text{m}$ in radius as medium-sized; and we consider large particles to be those having radii greater than $100\ \mu\text{m}$.

cloud formation and droplet growth to determine the composition, abundance, and distribution of cloud particles in brown dwarf atmospheres. In Section 3, we obtain modal cloud particle sizes for several representative cloud-forming species of high abundance for atmospheric models spanning a broad range of effective temperatures and surface gravities. In Section 4, we compare our particle sizes with those of two other recent papers that have also addressed clouds (Ackerman & Marley 2001, Helling *et al.* 2001). In Section 5, we apply our cloud model to brown dwarf spectra by computing the opacity of clouds resulting from the wavelength-dependent effects of Mie scattering and absorption of radiation. We also demonstrate the importance of clouds as an opacity source by comparing the spectrum of a cloudy brown dwarf atmosphere with that of a cloud-free atmosphere.

2. The Cloud Model

2.1. Condensation Level

The present cloud model follows much of the formalism of Lewis (1969), Rossow (1978), Stevenson & Lunine (1986), and Lunine *et al.* (1989). As in Lewis (1969), we compare the partial pressure of a given condensable species to its saturation vapor pressure. Only at levels where the partial pressure exceeds the saturation vapor pressure can condensation begin. However, the required level of supersaturation for efficient condensation depends on the physics of the nucleation process itself. We discuss the two relevant nucleation processes—homogeneous and heterogeneous nucleation—in more detail in Section 2.2. In a clean atmosphere, in which the availability of condensation nuclei is low (the case of homogeneous nucleation), condensation will not begin until the vapor becomes highly supersaturated. Thus, the partial pressure will greatly exceed—often by a factor of two or more—the saturation vapor pressure (Rogers & Yau 1989). This situation is expected to occur in methane clouds in Titan’s atmosphere (Tokano *et al.*, 2001). Thus, the condensation level appears where

$$P_{cond} > P_{sat} (1 + \mathcal{S}_{max}). \quad (1)$$

Here, P_{cond} is the partial pressure of the condensing vapor, and P_{sat} is its saturation vapor pressure. S_{max} in Equation 1 is the assumed maximum supersaturation, which appears in the calculation as an essentially free parameter, though we have some guidance as to its likely value from measurements of the supersaturation of water clouds on Earth. We assume in these calculations that the abundance of condensation nuclei is sufficient for heterogeneous nucleation to begin at only 1% maximum supersaturation, though we will explore the effect of this parameter on the computed particle sizes subsequently.

In addition to the original Lewis (1969) cloud model, we also treat the case of heterogeneous (or chemical) condensation, in which chemical constituents different in composition from the cloud react chemically to produce the condensate. For example, we allow Mg, Si, and O to produce forsterite, Mg_2SiO_4 . In such cases of heterogeneous condensation, the concept of a saturation vapor pressure is replaced by the heterogeneous condensation pressure. We apply the chemical equilibrium model of Burrows & Sharp (1999), along with their rainout prescription, to a solar-composition gas (Anders & Grevesse 1989) to determine which chemical species are energetically favored. The calculation determines the equilibrium compositions, in the presence of a gravitational field, by minimizing the Gibbs free energy of the system.

Figure 1 shows the condensation curve for two condensates, forsterite (Mg_2SiO_4) and gehlenite ($Ca_2Al_2SiO_7$), as well as the saturation vapor pressure curve of iron, and several model brown dwarf atmospheres. The intersection points between the four long-dashed curves of brown dwarf temperature-pressure profiles and the condensation curves of forsterite and gehlenite represent levels in the atmosphere at which the relevant species may appear via one or more chemical reactions.

The more familiar case of homogeneous condensation, or direct condensation from a vapor of the same composition, does occur for water and iron. Thus, for the condensation of iron and water, we follow Lewis (1969) and employ the well-known saturation vapor pressure relations of iron and wa-

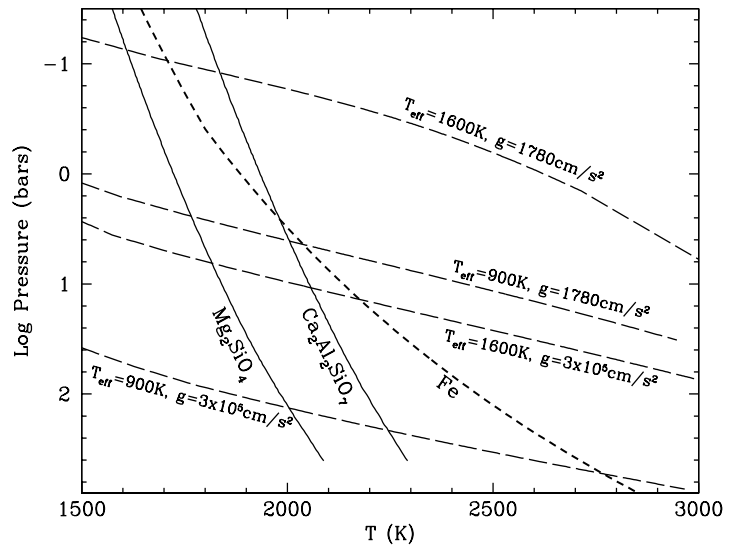


Fig. 1.— Illustrates the locations of the cloud bases for four different atmospheric models (long-dashed curves) and three different chemical species (solid and short-dash curves). The atmospheric models are at two different surface gravities and two different effective temperatures. The short-dashed curve defines the atmospheric pressures and temperatures for which the vapor pressure of Fe equals its saturation vapor pressure. This curve is obtained using the Fe saturation vapor pressure expression in Barshay & Lewis (1976). It uses an Fe mixing ratio (by number) equal to 5.4×10^{-5} , which is the maximum allowed mixing ratio for Fe at solar metallicity when H is all in the form of H_2 . The two solid lines are the curves which illustrate when condensation of forsterite (Mg_2SiO_4) and gehlenite ($Ca_2Al_2SiO_7$) become energetically favored. Thus, they represent the pressure dependent condensation temperatures of those species under the assumption that chemical equilibrium holds. The intersection of a given atmospheric model and the two condensation curves represents the pressures and temperatures at the bases of the chemically condensing clouds in our cloud model. However, for iron, the cloud base will be slightly offset from the intersection point if the iron vapor is significantly supersaturated (see Equation 1).

ter (Barshay & Lewis 1976, Lunine *et al.* 1989). In Figure 1, the iron curve is thus shown as a thick, short-dashed line, as a reminder that the iron cloud condenses directly from iron vapor.

2.2. Microphysical Timescales

Although the chemistry applying to brown dwarf atmospheres is radically different from Earth’s atmospheric chemistry, we nevertheless treat the various competing effects in the cloud formation process as microphysical timescales (Rossow 1978). In our model, five microphysical processes compete with gravitational fallout to increase the modal particle size: 1) convective uplifting of condensable vapor, 2) heterogeneous nucleation, 3) homogeneous nucleation, 4) coagulation, and 5) coalescence. Each process is characterized by a single-valued timescale which expresses its relative importance.

The τ_{fall} timescale represents gravitational fallout of particles, which is the fundamental process limiting particle growth. As the particles become large, they fall out. We take the gravitational fallout timescale to be the time required for particles to fall through a pressure scale height of the atmosphere at terminal velocity. The terminal velocity of falling particles depends on their size, their shape, and the nature of the fluid flow around them (e.g., Stokes flow or turbulent flow). We assume spherical particles throughout this paper. The sedimentation process thus depends on the particle radius and the physical properties of the atmosphere, including its density and viscosity.

The τ_{conv} timescale represents the convective upwelling of particles. Although convective upwelling is not itself a particle growth process, convective updrafts hold small cloud particles aloft in the atmosphere so that they accumulate more material via coagulation, coalescence, etc. Convective upwelling is proportional to the characteristic bulk upwelling velocity of the convecting fluid, and it therefore competes directly with the sedimentation velocity.

τ_{nuc} characterizes particle growth via homogeneous nucleation, in which highly supersaturated vapor condenses spontaneously due to rapid col-

lisions between the vapor molecules. This process is rarely observed to occur in nature because its timescale will be longer in almost all cases than τ_{cond} , which characterizes the condensation growth of a population of particles via heterogeneous nucleation. In heterogeneous nucleation, particles nucleate onto seed particles, called condensation nuclei, which are presumed to populate the region of condensation. As discussed, when heterogeneous nucleation is efficient, condensation may begin even when the level of supersaturation is quite low ($< 1\%$). Neither nucleation process represented by τ_{nuc} and τ_{cond} apply to the species—forsterite and gehlenite—which appear due to chemical reactions rather than from a supersaturated vapor. The nucleation timescale expressions apply only to the species—iron and water—for which the condensate forms directly from a vapor of the same composition. For chemically condensing species, we ignore growth by nucleation.

Coagulation and coalescence represent particle growth due to collisions. τ_{coag} refers to the formation of larger particles by the collision of smaller particles. It thus depends primarily on the thermal temperature, viscosity, and the number density of cloud particles. τ_{coal} characterizes the growth of particles by coalescence, in which large particles having high downward velocities in the fluid overtake and merge with small, slowly falling particles. Thus, coalescence refers to the collisional process caused by the different fall speeds of different sized particles, whereas coagulation is collisional growth resulting from Brownian motion.

The expressions for four of the microphysical timescales are computed in Rossow (1978) (his τ_{cond} , τ_{coal} , τ_{coag} , and τ_{fall}). Because these expressions depend on the values of both the Knudsen and Reynolds numbers, we compute these values during the particle growth phase of the calculation. The Knudsen number differentiates between the regimes—classical and gas kinetic—of physical interaction between cloud particles and the surrounding medium. It is defined by $\text{Kn} = \lambda/r$, where r is the cloud particle’s radius and λ is the mean free path of atmospheric gas particles. The condensation timescale given in Rossow (1978),

dominates over homogeneous nucleation. We relax this assumption by incorporating the process of homogeneous nucleation explicitly (τ_{nuc}). For the timescale of homogeneous nucleation, we have adapted expressions from Stevenson & Lunine (1988) for large Knudsen numbers:

$$\tau_{nuc} = \frac{P c_{sound} R_{gas} T}{r \rho_{cond} L^2 \mu [exp(2\epsilon_{surf} \mu / r R_{gas} T \rho_{cond}) - 1]} \quad (\text{Kn} > 1) \quad (2)$$

Here, r is the particle radius, ρ_{cond} is the mass density of the condensate, L is the latent heat of vaporization, μ is the mean molecular weight of the atmospheric gas mixture (g/mol), ϵ_{surf} is the surface tension of the condensed liquid molecules, c_{sound} is the sound speed in the atmosphere, and P and T are the ambient temperature and pressure.

The more common case of small Knudsen numbers, which corresponds to high atmospheric gas density, is a commonly used meteorological expression (see Rogers & Yau 1989). The low Knudsen number expression for τ_{nuc} is written in terms of the critical radius at which the equilibrium vapor pressure over the surface of a particle equals the ambient vapor pressure. The equilibrium vapor pressure over the surface of a liquid particle, because of its finite curvature, is in general higher than the equilibrium vapor pressure over a flat surface of the liquid, which is the saturation vapor pressure normally measured in the laboratory. Therefore, the critical radius of the liquid particle will only be attained when the saturation ratio exceeds unity; i.e., when the actual ambient pressure exceeds the saturation vapor pressure. The critical radius thus depends on the supersaturation \mathcal{S}_{max} :

$$r_c = \frac{2N_A m \epsilon_{surf}}{R_{gas} \rho T \ln(1 + \mathcal{S}_{max})}. \quad (3)$$

In Equation 3, N_A is Avogadro's number, m is the mass of a molecule of condensate in grams, and ρ is the mass density of the surrounding gas. The expression for τ_{nuc} , in terms of the critical droplet radius r_c then reads

$$\tau_{nuc} = \frac{1}{P} \sqrt{\frac{mk_b T}{2\pi r_c^4}} Z_n^{-1} exp\left(\frac{4\pi r_c^2 \epsilon_{surf}}{3k_b T}\right) \quad (\text{Kn} < 1). \quad (4)$$

In Equation 4, Z_n is the dimensionless Zeldovich or non-equilibrium factor, which equals 10^{-2} in

For the timescale of particle growth due to convective updrafts, we take $\tau_{conv} = H/v_{conv}$, where $H = R_{gas} T / \mu g$ is the atmospheric scale height in terms of g , the local gravity. The convective timescale is thus the time required for gas parcels to rise through a pressure scale height. The upward convective velocity, v_{conv} , is estimated via (Kn > 1) mixing length prescription in the atmosphere code.

2.3. Our Cloud Code

The code proceeds in two stages: (1) determination of the cloud base globally in the atmosphere, and then (2) particle growth at each atmospheric temperature-pressure level. The algorithm is run for each of the atmospheric temperature-pressure profiles, which differ in effective temperature and gravity, and for each condensable species separately.

In stage (1), two cases must be treated separately, as explained above. In the case of homogeneous condensation, we calculate the intersection between the partial pressure of the condensable vapor and its saturation vapor pressure curve, and identify the condensation level using Equation 1. In the case of heterogeneous condensation, in which the condensing chemical is not present in vapor form below the cloud base, we determine the cloud base by using the chemical equilibrium model of Burrows & Sharp (1999) (see Figure 1).

In stage (2), we calculate the modal size of particles, which are assumed to be spherical, at each atmospheric temperature-pressure level. The model outputs the modal particle radius. This radius is determined by growing an embryonic particle of radius $\sim 10 \text{ \AA}$ slowly until the various competing particle growth timescales are balanced by the timescale of gravitational fallout. Thus, for the optimal cloud particle, the sedimentation timescale equals the shortest of the growth timescales.

Our treatment of rainout, in which condensates settle gravitationally and thus become depleted from the upper atmosphere, is based on the assumption that all of the supersaturated vapor above the base of the cloud will condense. Because the material available for condensation is

limited by the partial pressure of the condensing gas (or gases), which can never exceed $(1 + \mathcal{S}_{max})$ of the saturation vapor pressure, the mass density of condensate drops off rapidly with height in the cloud. Thus, rainout is effective in all cases, and 100% of the atoms in the solar-composition gas that are initially available for condensation become sequestered in the condensate within a scale height of the atmosphere. For example, because the limiting atomic species for the formation of forsterite is magnesium, and forsterite is favored chemically below about 2000 K, magnesium will have rained out near the forsterite cloud level, and no magnesium will be available for further condensation into other chemicals high above the forsterite cloud level. Rainout thus depletes the atmosphere of the most refractory elements at progressively lower temperatures and pressures.

2.4. Free Parameters

In addition to \mathcal{S}_{max} , the assumed maximum supersaturation, the free parameters of the cloud model include the vapor mixing ratios and the sticking coefficients for coagulation and coalescence. The vapor mixing ratios have been calculated assuming solar (Anders & Grevesse 1989) abundances of the elements in the atmosphere.

Coagulation and coalescence are not expected to be 100% efficient in all cases, because some molecules stick together when they collide more easily than others. Therefore, we have divided the timescales for coagulation and coalescence, given in Rossow (1978) as τ_{coag} and τ_{coal} , by efficiency parameters ϵ_{coag} and ϵ_{coal} .

For condensation directly into solid particles, coalescence is extremely inefficient. This applies to forsterite and gehlenite because the solid phase is strongly favored once the temperature decreases sufficiently for the chemical to appear (see Figure 1). Therefore, for the heterogeneously condensing materials, we have ignored coalescence ($\epsilon_{coal} = 0$). For the species condensing into liquid particles (iron and water) we have taken $\epsilon_{coag} = 10^{-1}$ and $\epsilon_{coal} = 10^{-3}$ (Lunine *et al.* 1989). We have also used $\epsilon_{coag} = 10^{-1}$ for the coagulation efficiency of heterogeneously condensing species. Subsequently, we will argue that this choice is rel-

alescence generally operate more slowly, for the atmospheres we are considering here, than heterogeneous nucleation and convection. We discuss in Section 3.4 how varying these parameters affects the general features of the cloud.

3. Model Results

3.1. Modal Particle Sizes

We compute particle sizes for each of four species on a set of atmospheric models spanning the ranges $T_{eff} = 600 - 1600$ K and $g_{surf} = 1.78 \times 10^3 - 3 \times 10^5$ cm s⁻². We chose the most abundant condensable species in the solar-composition mixture: iron, forsterite, and water. Iron and forsterite are the most abundant high-temperature condensates (Lunine *et al.* 1989). Although we have included one of the calcium-aluminum silicates, gehlenite, and these refractory species do condense into clouds, their abundance in a solar-composition gas is lower than that of iron or forsterite by a factor of about ten (Lunine *et al.* 1989). Thus, the contribution of the calcium and aluminum silicates to the total opacity is expected to be relatively minor.

3.2. Trends With Brown Dwarf Gravity and Effective Temperature

Figures 2, 3, and 4 show the particle sizes computed by our model for a range of brown dwarf atmospheric profiles. Each circled point represents, for the atmospheric profile to which it applies, the grain size computed by our model at the initial cloud level (i.e., the cloud base). The atmospheric profile corresponding to each circled point can be ascertained from its position on the diagram: gravity increases from left to right, whereas effective temperature increases from bottom to top in the field. These graphs say nothing about the distribution of material above the cloud base; they apply only to the initial condensation level where the mass density of material is greatest. Figure 2 shows the results for iron grains, which condense directly from iron vapor. Figure 3 shows the analogous results for forsterite grains, which appear as a result of chemistry (i.e., heterogeneous condensation). Figure 4 shows the same for gehlenite,

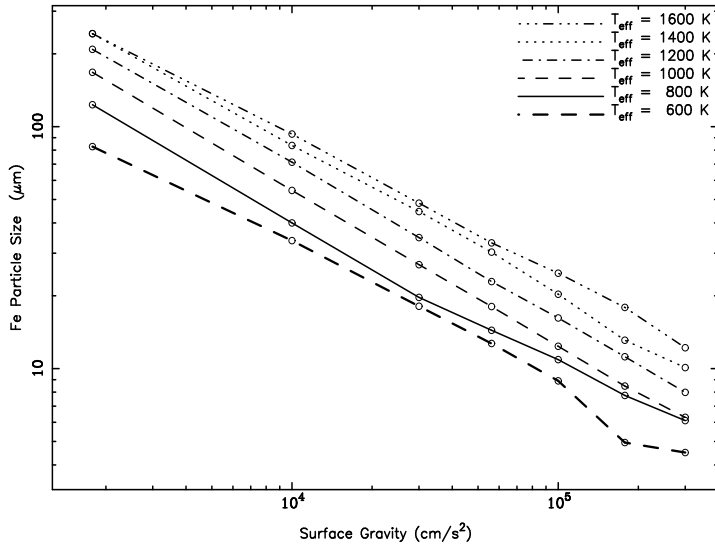


Fig. 2.— The grain sizes of iron (Fe) at the cloud base for a range of brown dwarf atmospheric temperature-pressure profiles. The figure displays the modal particle sizes obtained by applying the model described in Section 2 to each model brown dwarf atmosphere. The profiles span a range of effective temperatures and surface gravities from $T_{eff} = 600 - 1600$ K and $g_{surface} = 1.78 \times 10^3 - 3 \times 10^5$ cm s⁻². Each circled point corresponds to a different brown dwarf atmospheric profile whose effective temperature and gravity depend on the point's location in the field. The figure shows that high-gravity brown dwarfs will have characteristically smaller particle sizes than low-gravity brown dwarfs for a given effective temperature. Similarly, hotter brown dwarfs will exhibit larger particle sizes, for a given surface gravity, than cooler brown dwarfs.

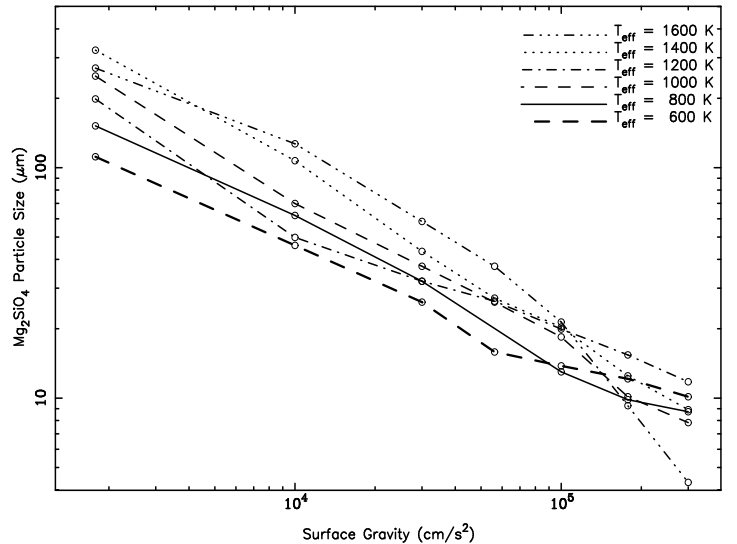


Fig. 3.— Companion to Figure 2: this shows similar trends for forsterite (Mg_2SiO_4) particle radii. The forsterite particles become extremely large ($\sim 500 \mu m$) in very low gravity objects. Because forsterite forms in abundance in the atmosphere, the optical effects of forsterite clouds are potentially very important, depending on the particle sizes.

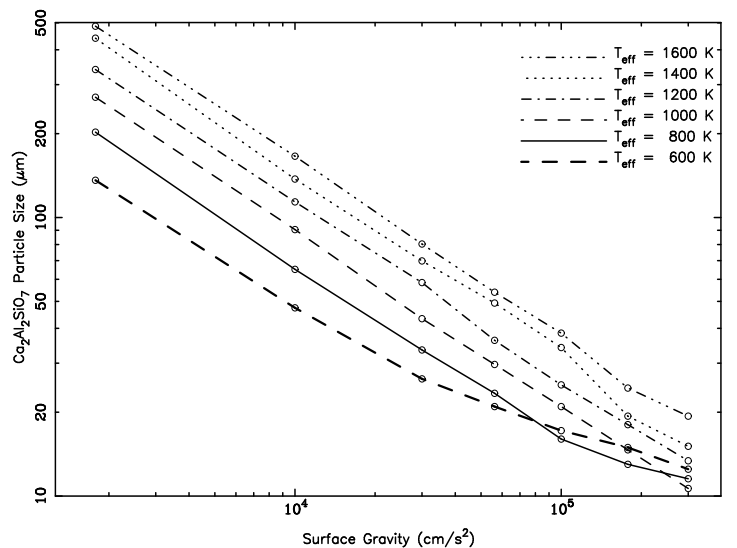


Fig. 4.— The particle size trends for the calcium-aluminum silicate gehlenite ($Ca_2Al_2SiO_7$). This species is less abundant than forsterite by ~ 10 , but it has the important effect of sequestering Ca and Al in condensed form below the photosphere of the cooler objects.

Figures 2, 3, and 4 show that cloud grains in hot brown dwarfs, for a fixed surface gravity, are systematically larger than in cold brown dwarfs. Similarly, cloud particles in objects with high surface gravities, for a fixed effective temperature (e.g., older brown dwarfs), are systematically smaller than in objects having low surface gravities.

The trend with surface gravity is simple to explain: particles settle more quickly in high-gravity environments. This appears to be the overriding effect governing particle size. Although both the atmospheric pressure and temperature at the cloud base are higher in high-gravity objects, and the convection therefore more rapid, gravity dominates and the resulting particles are smaller. For the lowest gravity objects, the forsterite particles grow quite large. They thus contribute only negligibly to the total optical depth (Sudarsky *et al.* 2000).

The trend with effective temperature results from the difference in convective updraft velocity between colder and hotter objects. Objects with higher effective temperatures must transport a higher flux of thermal energy to the surface via interior turbulent convection. Therefore, the updrafts holding cloud particles aloft will be more rapid in the higher T_{eff} objects, resulting in larger particle sizes.

3.3. Cloud Decks in Convective vs. Radiative Regions

Brown dwarfs are almost fully convective, with only a thin radiative atmosphere (Basri *et al.* 2000, Burrows *et al.* 2001). Convective uplifting sustains the particles against gravitational fallout. The effectiveness of this process depends on the velocity scale of the convection. Hence, the gradient in the convective velocity plays a role in determining particle size. Deep in the atmosphere, the brown dwarf is fully convective, with a relatively high updraft velocity (approaching 50 m/s). At higher altitudes, the updraft speed is small or zero. Therefore, clouds at depth are convective; clouds at altitude are quiescent. By quiescent, we mean clouds formed in convectively stable layers.

Particles in quiescent clouds are generally smaller than particles in convective clouds. Figure 5 compares the particle sizes of condensed iron for a brown dwarf model having $T_{eff} = 1500$ K and $g_{surf} = 5.62 \times 10^4$ cm s⁻². The distribution of particle sizes throughout the cloud, which extends roughly an atmospheric scale height from base to top, is shown for iron under two contrasting assumptions: (1) the cloud is convective (i.e., $\tau_{conv} = H/v_{conv}$), and (2) the cloud is radiative (i.e., $\tau_{conv} = \infty$). Our calculations suggest that for this atmosphere, a convective iron cloud is more realistic. We thus predict the solid curve for the actual particle size distribution in the cloud deck. Figure 5 compares the particle sizes obtained by activating and deactivating the convective uplifting mechanism.

Figure 5 shows, for this particular brown dwarf atmosphere, that cloud particles growing primarily as a result of convective upwelling are largest near the cloud base but then diminish rapidly with height. This decrease in size is due to the proximity of the iron cloud base, for this particular model, to the radiative-convective boundary of the atmosphere where the gradient in the upwelling velocity is steep. For convective clouds deep within the convective zone where the upwelling velocity is nearly constant, the particle sizes will be more constant throughout the cloud deck. However, deep clouds will not strongly influence the object's emergent spectrum.

If the cloud is radiative, the particles will not grow as large as they would under the influence of convection. Furthermore, their sizes will not decrease by more than a factor of two from base to cloud top. This result appears quite general for the radiative clouds we have investigated.

The structure of the cloud decks (e.g., as shown in Figure 5) of brown dwarfs is crucial for computing the optical depth of the cloud. For clouds in which the overall particle sizes decrease significantly with altitude above the cloud base, it may be that the bulk of the optical depth in the near-infrared will be contributed not by the lowest cloud layers but by intermediate layers having significant abundances of smaller particles.

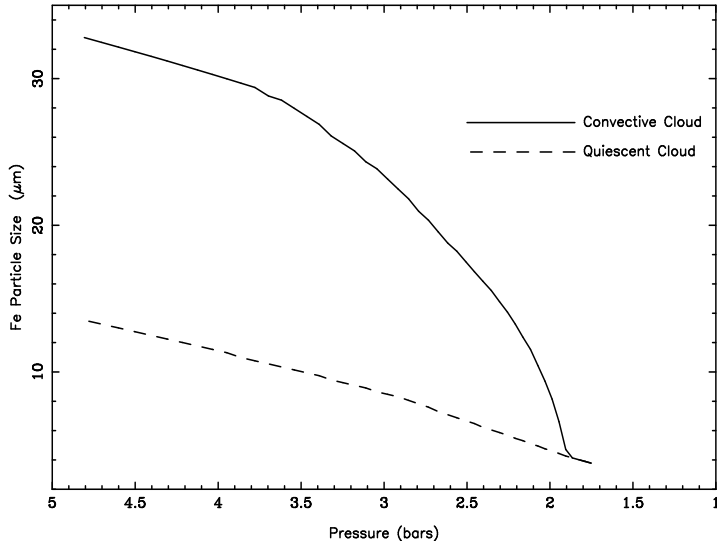


Fig. 5.— The structure of an iron cloud deck for a particular brown dwarf at $T_{eff} = 1500$ K and $g_{surface} = 5.62 \times 10^4 \text{cm s}^{-2}$ assuming a constant 1% maximum supersaturation during the entire particle growth phase. The dashed curve assumes that convection is not effective at sustaining particle growth. Therefore, the particles do not grow as large. For this radiative (or quiescent) cloud, the particle sizes vary by about a factor of two within an atmospheric scale height (above which very little condensable material remains). On the other hand, for the convective cloud, in which we allow updrafts to sustain particle growth against gravitational sedimentation, the particles grow relatively large. Because the cloud base is slightly above the radiative-convective boundary of the profile, the updraft velocity decreases rapidly with height. Thus, for clouds forming near unity optical depth, we expect variable particle sizes from the base to cloud top. The cloud particle size distribution of the convective cloud merges with the distribution for a quiescent cloud once the updraft velocity becomes negligible.

3.4. Varying the Free Parameters

Among the model free parameters discussed above, the level of maximum supersaturation is the most problematic. \mathcal{S}_{max} is particularly difficult to calculate independently, and because the condensation timescale depends on it, \mathcal{S}_{max} has a significant effect on the resulting particle size. This effect will be manifest in quiescent clouds, but will be less important in convective clouds because, in rapidly convecting regions, convective upwelling can directly sustain particle growth.

Figure 6 shows, for one brown dwarf model, the effect of varying \mathcal{S}_{max} on the modal particle size of a water cloud. For low levels of supersaturation, the particles grow to a radius of $\sim 50 \mu\text{m}$. In this case, abundant condensation nuclei raise the rate of heterogeneous nucleation high above the rate of homogeneous nucleation, and condensation can begin as soon as the atmosphere becomes saturated. For high levels of supersaturation ($>10\%$), they grow much larger, to $\sim 150 \mu\text{m}$. In this clean atmosphere case, heterogeneous nucleation does not occur, and the partial pressure of water in the atmosphere must greatly exceed the saturation vapor pressure in order for condensation to begin. We have assumed an intermediate value of $\mathcal{S}_{max} = 10^{-2}$ for iron. This value is our best guess for the \mathcal{S}_{max} of vaporous Fe based on a knowledge of the maximum supersaturations attained in terrestrial water clouds (Rossow 1978).

The other free parameters of the cloud model are less difficult. The mixing ratios depend on the metallicity, which we have taken to be solar. The chemical equilibrium code requires the metallicity to be specified. Once the assumption of elemental composition is made, however, we can calculate the partial pressures of all the gases in the mixture. We defer a discussion of the effect of brown dwarf metallicity on cloud structure to future work.

The efficiency parameters for coagulation and coalescence, ϵ_{coag} and ϵ_{coal} , are potentially important. However, our model results show that the timescales of these processes, whatever their efficiency, are consistently longer than the timescale of growth by heterogeneous nucleation at 1% supersaturation. The model suggests that coales-

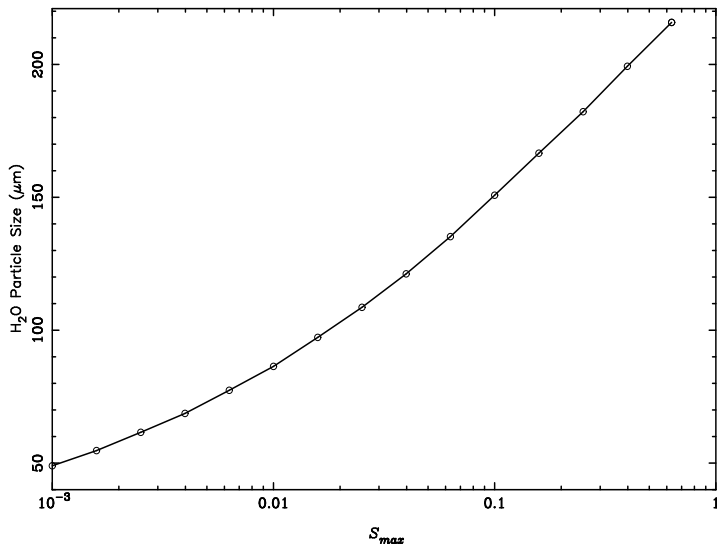


Fig. 6.— The modal particle sizes, as a function of S_{max} , for a water cloud in the upper atmosphere of a cool brown dwarf: $T_{eff} = 350$ K and $g_{surface} = 10^4 \text{cm s}^{-2}$. Convection is not occurring in these outer layers. The figure shows the difficulty in estimating particle sizes for radiative clouds because of the strong dependence on assumed maximum supersaturation. Water cloud particles will grow extremely large in a clean atmosphere; i.e., one in which the paucity of condensation nuclei requires high levels of supersaturation of the vapor in order for nucleation to begin. In this case, nucleation proceeds rapidly and the particles grow very large. For convective clouds, on the other hand, the value assumed for the maximum supersaturation is not important, as the cloud particles will grow to nearly the same size for any value of $S_{max} < 100\%$.

species—iron and water—in which coalescence operates efficiently. Coalescence, for the largest particles we have grown ($\sim 500 \mu\text{m}$), can approach the timescale of heterogeneous nucleation. However, for the clouds in most of the atmospheres we have treated, coalescence is still slower than heterogeneous nucleation by a factor of ten or more. Indeed, unless the efficiency of coalescence is greater than one, requiring charged aerosols (Rossow 1978), coalescence will never dominate the distribution of particles.

4. Comparison With Other Cloud Models

4.1. Ackerman & Marley (2001)

Ackerman & Marley (2001) also employ a particle growth algorithm based on microphysical timescale expressions. However, they introduce an additional parameter, f_{rain} , which characterizes the vertical distribution of condensate in the cloud. The f_{rain} parameter, as Ackerman & Marley (2001) state, is difficult to calculate from basic principles. They leave it as an adjustable parameter in their model. It depends on the mass-weighted sedimentation velocity of the cloud droplets and the convective velocity scale. The difficulty in calculating f_{rain} lies in the complexity of modeling fully the nature of the convection within the cloud. This problem has yet to be successfully attacked for brown dwarf atmospheres.

However, if it can be computed for these convective clouds, knowledge of f_{rain} can potentially provide a more realistic measure of the height and distribution of material in the cloud. For quiescent clouds, f_{rain} does not play a role. Ackerman & Marley (2001) have assumed $f_{rain} = 2-3$ in their calculations. This *ad hoc* choice of $f_{rain} > 1$ leads to a more compact cloud deck in which the condensable material is fully depleted within a third of an atmospheric scale height above the condensation level. By contrast, our cloud decks generally extend a full scale height above the cloud base (see Figure 5).

The particle sizes we obtain compare favorably with the sizes predicted by the Ackerman & Marley (2001) model. They predict modal particle radii in the intermediate size range of 40-80 μm for

with the particle size ranges shown in Figures 2, 3, and 4.

4.2. Helling *et al.* (2001)

Helling *et al.* (2001) study the onset of cloud particle growth via acoustic waves. They show that small ($1 - 10 \mu\text{m}$) sized particles can nucleate rapidly, normally within a few seconds. These values are consistent with our particle sizes in radiative regions under the assumption of zero supersaturation ($\mathcal{S}_{max} = 0$). Our larger particles form from continued nucleation and convective uplift. The grains generated in Helling *et al.* (2001) appear and disappear too rapidly to grow to the maximum size allowed gravitationally. In the present model, once Equation (1) is satisfied, the condensed phase is favored energetically, and the particles will continue to grow for minutes—even hours—before the available condensable material is used up. Therefore, by not including continued nucleation growth and the onset of coagulation and coalescence, Helling *et al.* (2001) systematically underestimate the particle sizes relevant to SMO atmospheres.

5. Discussion

5.1. Cloud Opacity

The effects of clouds on the emergent spectra of substellar objects depend strongly on grain sizes. We derive the wavelength-dependent absorption and scattering opacities of grains with a full Mie theory approach utilizing the formalism of van de Hulst (1957) and Deirmendjian (1969).

Figure 7 shows the results of such a calculation for forsterite grains in a brown dwarf atmosphere ($T_{eff} = 1500 \text{ K}$, $g_{surf} = 10^5 \text{ cm s}^{-2}$) based on our cloud model results and optical constants from Scott & Duley (1996). Also shown are the results for a larger grain size distribution peaked at 50 microns, as well as for a size distribution peaked at 0.1 microns, which is representative of an interstellar particle size (Mathis *et al.* 1977) often assumed to be appropriate for substellar objects (Allard *et al.* 2001; Barman *et al.* 2001). For comparison, we have plotted the atomic and molecular gaseous opacities (Burrows *et al.* 2001

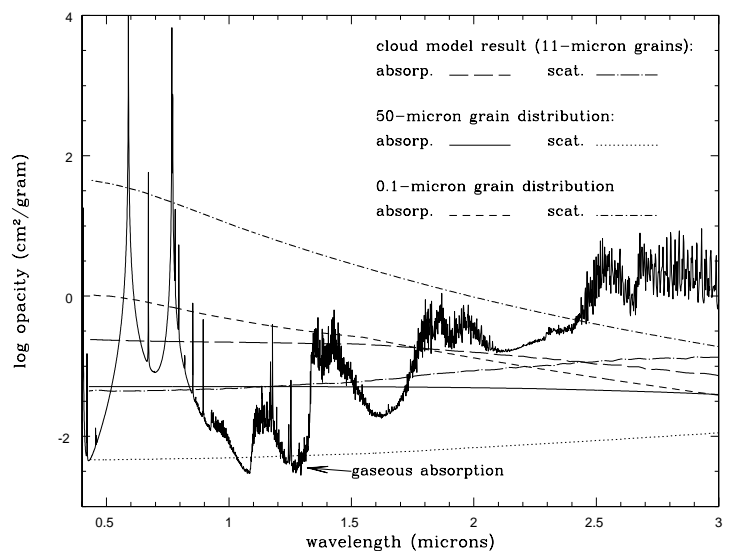


Fig. 7.— Scattering and absorption opacities of forsterite are compared with gaseous atomic and molecular absorption at 1600 K. Our modeled modal particle size, $11 \mu\text{m}$, in a brown dwarf ($T_{eff} = 1500 \text{ K}$, $g = 10^5 \text{ cm s}^{-2}$) is contrasted with both a larger size distribution peaked at $50 \mu\text{m}$ and a smaller size distribution peaked at $0.1 \mu\text{m}$. The $0.1 \mu\text{m}$ distribution is representative of an interstellar grain size assumed by some researchers. In all cases, a functional form of the distribution about the modal size is used (Deirmendjian 1964).

and references therein) at a temperature and pressure within the cloud region (1600 K, 2.5 bars). The substantial absorption and scattering differences between the size distributions, and relative to the gaseous absorption, convey the importance of proper cloud modeling.

5.2. Effect on Spectra

Figure 8 depicts the effects of our modeled forsterite cloud on the emergent spectrum of a brown dwarf ($T_{eff} = 1500\text{K}$, $g_{surf} = 10^5 \text{ cm s}^{-2}$). For this atmosphere model, obtained using a Feautrier code with accelerated lambda iteration (ALI) (Hubeny & Lanz 1995), the cloud extends about one pressure scale height. Its base resides at approximately 4 bars and 1800 K, the highest temperature in this atmosphere at which forsterite grains can form. A cloud-free model of the same effective temperature and gravity is plotted for comparison. Within the B ($\sim 0.45 \mu\text{m}$) and Z ($\sim 1 \mu\text{m}$) bands, the emergent flux is lowered by as much as one dex. However, the strong absorption by the wings of the sodium and potassium resonance lines is mitigated somewhat due to the clouds. Also of interest are the differences in the J ($\sim 1.25\mu\text{m}$), H ($\sim 1.6\mu\text{m}$), and K ($\sim 2.2\mu\text{m}$) infrared bands. The presence of clouds reduces the emergent flux in the otherwise relatively clear J and H bands, allowing more flux to escape between these bands and at longer wavelengths. In fact, the $J-K$ colors differ by over 1.5 magnitudes between the cloudy and cloud-free models.

6. Conclusions

6.1. General Results

In this article, we address the condensation and subsequent growth of cloud particles in the atmospheres of brown dwarfs. We present optimal particle sizes for three abundant species—iron, forsterite, and gehlenite—for a broad range of brown dwarf effective temperatures and surface gravities.

High-gravity brown dwarfs exhibit clouds with typical particle sizes in the $5 - 20 \mu\text{m}$ range. The particles grow much larger, however, in low-gravity objects, often greater than $100 \mu\text{m}$ in ra-

dius. We discovered a similar trend with effective temperature: hot brown dwarfs have characteristically larger particle sizes than cool brown dwarfs because of the increased energy flux that must be transported by convection. The distribution of cloud particle sizes depends strongly on the atmospheric parameters, and it is therefore unrealistic in spectral models to assume a single particle size distribution for the entire class of SMOs.

We demonstrate that particle size crucially affects the optical depth of the cloud. Unlike clouds having a particle size distribution centered at $0.1 \mu\text{m}$, these cloud decks do not dominate the opacity. Rather, they smooth the emergent spectrum and partially redistribute the radiative energy (see Figure 8).

6.2. Improved Cloud Models: Morphology and Patchiness

A complete theory of brown dwarf and giant planet atmospheres will require detailed modeling of clouds. Although obtaining plausible particle sizes is a good start, we have been unable to say anything yet about the morphology or patchiness of clouds. For example, on Jupiter, clouds appear in banded structures that vary latitudinally, while Neptune and Uranus show less latitudinal banding in their surface cloud patterns. The structure and patchiness of clouds on brown dwarfs is not known, though the putative variability detected by Bailer-Jones & Mundt (2000) suggests that cloud patches are not necessarily static.

A simple approach to understanding surface cloud distributions is the moist entraining plume model. Such a model has been put forth by Lunine *et al.* (1989) based on the work of Stoker (1986) for Jupiter’s equatorial plumes. The model generates plumes from atmospheric material whose buoyancy is increased by the release of latent heat from condensation.

More elaborate calculations would involve three-dimensional modeling of the general atmospheric circulation with detailed physics of convecting material. Such an approach will be quite difficult to implement.

6.3. Future Work in Spectral Synthesis

The results of the current work will be useful in developing more elaborate spectral models of substellar atmospheres. We plan to follow up the present work with an exploration of the spectral effects of a variety of cloud compositions and distributions. Although Figure 8 shows the general effects of introducing a forsterite cloud on the spectrum of a brown dwarf, we have not yet varied the particle size distribution from the base to the top of the cloud. A large drop in the particle sizes with height above the cloud base will produce greater optical depth than a cloud deck having uniformly large particles. It is also likely that clouds of more than one species will form near the photosphere simultaneously. The wavelength-dependent indices of refraction of many compounds are not that well known. Thus, a major future challenge will be cataloging the optical properties of the major condensates and incorporating them self-consistently into substellar model atmospheres.

We thank Ivan Hubeny, Chris Sharp, Jonathan Fortney, Jason Barnes, Bill Hubbard, Jim Liebert, and Michael Meyer for insightful discussions and advice. This work was supported in part by NASA grants NAG5-10450, NAG5-10760 and NAG5-10629.

REFERENCES

- Ackermann, A. & Marley, M.S. 2001, ApJ, 556, 872
- Anders, E. & Grevesse, N. 1989, Geochim. Cosmochim. Acta, 53, 197
- Allard, F., Hauschildt, P. H., Alexander, D. R., Tamanai, A., & Schweitzer, A. 2001, Astrophysical Journal, 556, 357
- Barman, T., Hauschildt, P. H., & Allard, F. 2001, Astrophysical Journal, 556, 885
- Bailer-Jones, C.A.L., & R. Mundt, 2000, Astron. Astrophys. , 374, 107
- Barshay, S.S., & Lewis, J.S. 1976, Ann. Rev. Astr. Ap., 14, 81
- Basri, G. 2000. Annu. Rev. Astron. Astrophys.,
- Burrows, A. & Sharp, C.M. 1999, ApJ, 512, 843
- Burrows, A., Hubbard, W.B., Lunine, J.I., and Liebert, J. 2001, Rev. Mod. Phys., July 2001
- Burrows, A., Marley, M., Hubbard, W. B., Lunine, J. I., Guillot, T., Saumon, D., Freedman, R., Sudarsky, D. & Sharp, C. 1997, ApJ, 491, 856
- Deirmendjian, D. 1964, Applied Optics, 3, 187
- Deirmendjian, D. 1969, *Electromagnetic Scattering on Spherical Polydispersions* (New York: American Elsevier Publishing Company, Inc.), 17
- Helling *et al.* 2001, Astron. Astrophys. , 376, 194
- Hubeny, I. and Lanz, T. 1995, ApJ, 439, 875
- Jones, H.R.A. and Tsuji, T. 1997, ApJ, 480, L39
- Kirkpatrick *et al.* 1999, ApJ, 519, 802
- Legett *et al.* 1999, Astrophys. J. Lett., 517, L139
- Lewis, J.S. 1969, Icarus, 10, 365
- Lunine *et al.* 1989, ApJ, 338, 314
- Rogers, R.R., and Yau, M.K. 1989, *A Short Course in Cloud Physics, Third Edition* (Woburn, MA: Butterworth-Heinemann)
- Rossow, W. B. 1978, Icarus, 35, 1-50
- Scott, A. & Duley, W. W., Astrophysical Journal Supplements, 105, 401
- Stevenson, D.J., and Lunine, J.I., 1988, Icarus, 75, 146
- Stoker, C.R., 1986, Icarus, 67, 106
- Sudarsky, D., Burrows, A., and Pinto, P. 2000, ApJ, 538, 885
- Tokano, T., Neubauer, F.M., Laube M., and McKay, C.P. 2001, Icarus, 153, 130T
- van de Hulst, H. C. 1957, *Light Scattering by Small Particles* (New York: Dover Publications, Inc.), 114

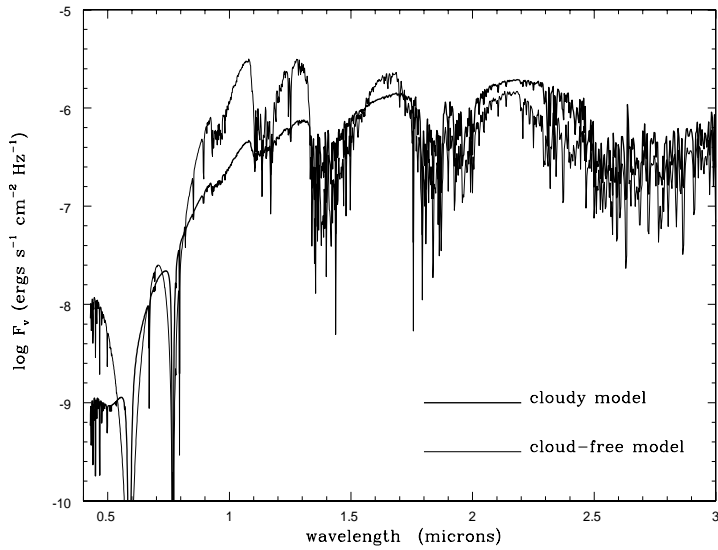


Fig. 8.— The emergent spectrum of a cloudy brown dwarf ($T_{\text{eff}} = 1500 \text{ K}$, $g = 10^5 \text{ cm s}^{-2}$) is compared with a cloud-free model of the same effective temperature and gravity. In the cloudy model, the base of the forsterite cloud resides at approximately 4 bars (1800 K) and extends roughly one pressure scale height. Within the cloud region, the full solar abundance of magnesium has been condensed into forsterite grains.